# Pump-Polarization Effects in Dye-Doped Polymer Optical Fibers

M. Asunción Illarramendi, Joseba Zubia, Inaki Bikandi, Igor Ayesta, Itxaso Parola, Ibon Aramburu, Jon Arrue, Akihiro Tagaya, and Yasuhiro Koike

***Abstract*—This paper presents a study on the influence of the polarization of the pump beam on the emission properties of dye-doped polymer optical fibers. The fiber samples, which are pumped transversely with linearly polarized light, are graded-index polymer optical fibers doped with rhodamine 6G. The variation of the intensity and angular distribution of the output emission are theoretically and experimentally analyzed as the polarization direction of the pump is changed. The analysis is carried out both in the regime of fluorescence and in the regime of amplified spontaneous emission. It is shown that a pump polarization perpendicular to the fiber symmetry axis yields not only higher emission efficiency but also narrower axial angular width. The effect of the polarization of the pump beam on the properties of the amplified spontaneous emission is also measured, including its threshold-like energy, relative efficiency, and optical gain. The results indicate that the pump polarization determines the light-emitting performance of dye-doped polymer optical fibers.**

***Index Terms*—Amplified spontaneous emission, doped polymer optical fibers, polarization, polymer light sources.**

## I. Introduction

IN THE last few years, there has been a growing interest in the field of photonics in relation with the incorporation of functional materials into solid-state organic hosts, especially into polymer optical fibers (POFs) [1], [2]. The feasibility of doping POFs with a wide range of materials has enabled new applications of POFs as active devices in the fields of lasers, amplifiers, switches, sensors, illuminators and luminescent solar concentrators in the visible region [2]–[5]. There are several well-known advantages of using POFs as host matrices. Compared with glass fibers, POFs offer easy and cheap manufacturing technology, high safety, and extremely high flexibility [6], [7]. Since POFs have much lower manufacturing temperatures than glass fibers, it is possible to embed a great variety of dopants in the fiber core, from organic dyes and conjugated polymers to other types of materials such as rare-earth ions, quantum dots or nanoparticles of noble metals. Moreover, the waveguide geometry of optical fibers provide a symmetric output beam profile with straightforward connectivity, optical confinement in the fiber core together with long interaction distances between light and active material, and a high ratio of surface area to volume, which makes heat dissipation more efficient.

Fiber light sources can be obtained by just pumping dye-doped POFs, due to the phenomenon called amplified spontaneous emission (ASE). This occurs because the spontaneous emission is partly guided along the fiber, and it is amplified by stimulated emission when the optical gain exceeds the optical losses caused by self-absorption, light scattering from fiber imperfections, and other factors [2]. ASE combines properties of laser radiation, such as relatively high intensity and directionality, with a low coherence and a broader bandwidth. These properties make doped POFs simply by themselves suitable to be used as broadband fiber sources in a wide range of applications, such as spectroscopy, low-coherence interferometry, sensing, and imaging [8]–[10]. They can also be employed as sources for fiber gyroscopes and for applications that need a broad spectral gain, such as the amplification of all the channels in a wavelength-division-multiplexing system [11]. Nowadays, ASE-gain properties of polymer doped nanofibers are being investigated for their use as light emitters in the fields of nanophotonics and optoelectronics [12], [13]. Generally, graded-index (GI) POFs are preferred to step-index (SI) ones. In GI doped POFs, the highest power density is located in the same region as the highest dye concentration, namely in the proximity of the fiber symmetry axis [2], [14], so the interaction between light and dopant is stronger and, consequently the output energy that can be obtained with GI POFs is greater than that achievable with SI POFs for the same pump energy. The optimum efficiency of these fiber light sources of ASE radiation does not only depend on the type of fiber, dopant employed and dopant concentration, but on the pumping characteristics as well. Contrary to POFs working as optical amplifiers, where the pump

Manuscript received November 24, 2017; revised June 27, 2018; accepted July 15, 2018. Date of publication July 23, 2018; date of current version August 8, 2018. This work was supported in part by the Fondo Europeo de Desarrollo Regional (FEDER), in part by the Ministerio de Economía y Competitividad under Project TEC2015-638263-C03-1-R, in part by the Gobierno Vasco/Eusko Jaurlaritza under Projects IT933-16, and in part by ELKARTEK under Grants KK-2016/0030, KK-2017/00033, KK-2017/00089, and KK-2016/0059. *(Corresponding author: M. Asunción Illarramendi.)*

M. A. Illarramendi, I. Parola, and I. Aramburu are with the Department of Applied Physics I, BIE/EIB, University of the Basque Country (UPV/EHU), Bilbao 48013, Spain (e-mail: ma.illarramendi@ehu.eus; itxaso.parola@ehu.eus; ibon.aramburu@ehu.eus).

J. Zubia, I. Bikandi, and J. Arrue are with the Department of Communications Engineering, BIE/EIB, University of the Basque Country (UPV/EHU), Bilbao 48013, Spain (e-mail: joseba.zubia@ehu.eus; inaki.bikandi@ehu.eus; jon.arrue@ehu.eus).

I. Ayesta is with the Department of Applied Mathematics, BIE/EIB, University of the Basque Country (UPV/EHU), Bilbao 48013, Spain (e-mail: igor.ayesta@ehu.eus).

A. Tagaya and Y. Koike are with the Faculty of Science and Technology, Keio University, Yokohama 223-8522, Japan (e-mail: akihiro_tagaya@nifty.com; koike@appi.keio.ac.jp).

Color versions of one or more of the figures in this paper are available online at http://ieeexplore.ieee.org.

Digital Object Identifier 10.1109/JLT.2018.2858447

0733-8724 © 2018 IEEE. Personal use is permitted, but republication/redistribution requires IEEE permission.
See http://www.ieee.org/publications_standards/publications/rights/index.html for more information.

light is usually injected longitudinally at one of the fiber ends, in doped POFs working as light sources of ASE radiation the pumping scheme is usually transverse, i.e., perpendicular to the fiber symmetry axis from the side [14]–[18]. In this scheme, not all the pump energy impinging from the side is absorbed as it crosses the fiber transversely. The absorbed fraction depends on the pump energy and on the excited length, and it could be as high as 80% in some cases [18]. Although a fraction of pump energy is lost, the method of side pumping presents some advantages, such as a greater control of the gain in the active volume [17], [18]. In addition, the optical losses determined by using the side-illumination technique [7], [19] and the ASE gains determined by using the variable-stripe-length (VSL) method [7], [20] are measured by pumping the doped POFs transversely. These non-destructive methods based on transverse excitation have proved to be a very useful tool to determine the optical characteristics in doped fibers.

Although polarization effects in solid-state organic devices of several geometries, such as polymer cylindrical microresonators or polymer thin films, have been extensively reported [21]–[26], many of these effects are generally poorly known in light sources based on doped POFs [7]. In this sense, and although doped POFs have been widely studied, the pump polarization employed is not mentioned in any of the works that use transverse pumping. In this work, we analyze the influence of the polarization of the pump beam on the characteristics of both the fluorescence and the ASE generated in GI POFs doped with rhodamine 6G that are pumped transversely with linearly polarized light. In particular, we have analyzed, theoretically and experimentally, the effect of the pump polarization on the emitted intensity and on the angular distribution of the emission around the fiber symmetry axis. The dependence on pump polarization of ASE properties, such as threshold-like energy, relative efficiency and optical gain, has also been experimentally measured.

The paper is organized as follows. The experimental techniques and the samples analyzed are described in Section II. The theoretical model that describes the variation of the light intensity and the angular distribution of the emission as a function of the polarization angle is explained through Section III. The comparison between experimental and theoretical behaviors together with the measured ASE performance are shown and discussed in Section IV. Finally, the summary of the work is presented in Section V.

## II. Experimental Details

Figure 1 shows the experimental set-up employed to measure the output emission from the fiber by pumping a stripe of light onto its side. The pump light employed was the pulsed output of a frequency-doubler of a Nd:YAG laser (EKSPLA NL301HT, 532 nm and pulse width ~20 ns). The pulse energy was controlled by inserting calibrated neutral density filters into the beam path. This was expanded and collimated using a divergent lens (L1) and a convergent lens (L2). The cylindrical lens (L3) in Fig. 1 was used for light to impinge onto the fiber side as a stripe beam. The dimensions of the illuminated area were a height of up to 1 mm and a width of size $z_e$. In all the measurements, the emitted light always propagates through a non-excited length $z_{ne}$ of at least 3.2 cm before reaching the detector, due to the size of the SMA connector at the fiber end. The electric-field polarization of the pump was controlled by two Glan-Laser Calcite polarizers with high resistance to laser damage, P1 and P2, (Newport 10GL08AR.14) and by a zero-order precision half-wave plate $L_{\lambda/2}$ (Newport 05RP32-532).

The angular distribution of the emission around the fiber symmetry axis (*z*-axis) has been obtained by analyzing its far-field pattern (FFP) provided by a Hamamatsu LEPAS-12 optical-beam-measurement system adjusted in the visible region. The analysis of the FFP images provides the angular distribution of the output emission around the fiber symmetry axis (*z*-axis). We have determined the sine of the angle at which the far-field angular intensity distribution falls by half, which will be called $(sin\,\theta_z)_m$. This gives an indication of average axial angle of the generated emission. This angle must not be confused with the critical angle or maximum acceptance angle for the generated emission in the fiber, which quantifies the coupling of the generated emission into non-refracting directions in the fiber [27], [28]. For the measurement of the emission spectra, we employed a fiber-optic spectrometer (Ocean Optics USB4000, with an optical resolution of 1.5 nm in the full width at half maximum). The optical gains of the fibers were calculated by employing the VSL method, in which the emission from the fiber is measured for a set of values of the illuminated length $z_e$ in the range between 0 and a certain maximum excitation length $(z_e)_{\max}$ [18]. $z_e$ was adjusted by means of a sliding blade (SB) that was located in the path between the pump laser and the fiber, and which could be moved stepwise by using a linear motor (see Fig. 1).

The fibers analyzed are GI poly(methyl methacrylate) (PMMA) POFs doped with rhodamine 6G in the fiber core. The fibers were manufactured using the interfacial-gel polymerization technique [29]. The radius of the fiber core is 0.3 mm and the total fiber radius including the cladding is 0.5 mm. In these fibers, the decrease of the core refractive index from the maximum value $n_{core}$ at the fiber axis to the minimum one $n_{clad}$ at the core-cladding interface is the typical one of a GI POF [18]. The dopant concentration is also non-uniform, with higher concentration near the fiber symmetry axis (see Fig. 2). Fiber samples with two different average concentrations of rhodamine 6G in the fiber core have been studied (12 ppm and 16 ppm). The length of these samples ranges between 15 cm and 20 cm. For the measurements, the fiber ends were carefully polished by hand with polishing papers.

## III. Theoretical Modeling

In the side-illumination technique, the fiber is illuminated from its lateral side and the generated light intensity is detected at one of the fiber ends. An illustration of the excitation used has been plotted in Fig. 3, which shows that the pump beam propagates along the direction of the *x*-axis and impinges on the lateral surface of the fiber. The lateral height of the incident beam relative to the plane *xz* containing the fiber symmetry

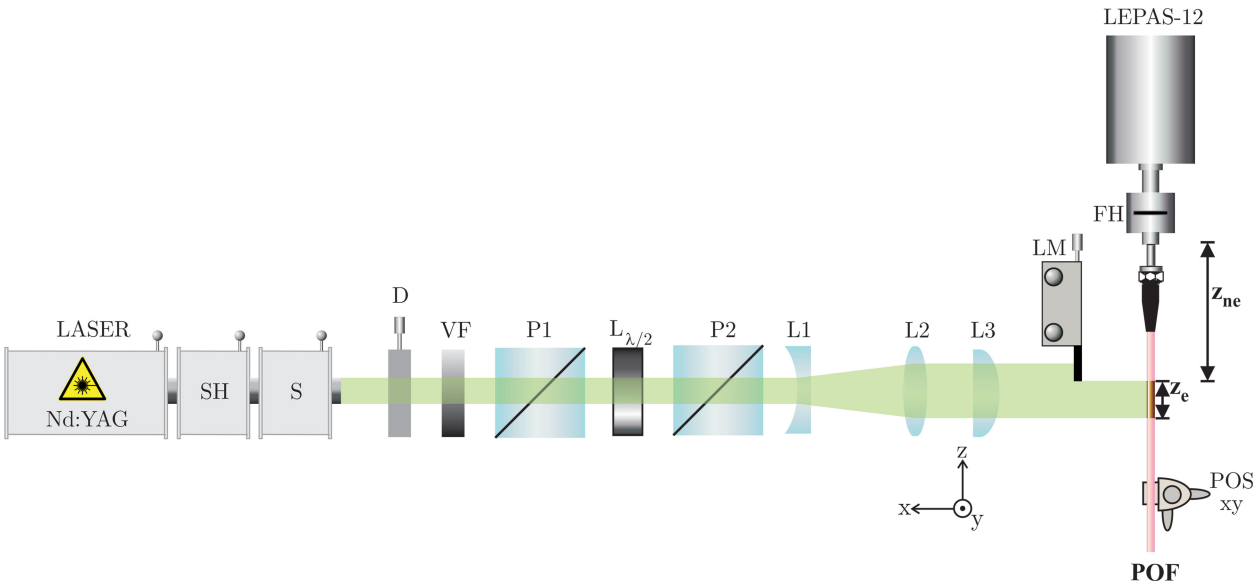


Fig. 1. Experimental setup used to measure the output emission in doped POFs. Legend: Nd:YAG: Laser; SH: Second harmonic generator; S: Harmonic beam separator; D: Diaphragm; VF: Variable absorptive neutral-density filter; P1, P2: Glan-laser calcite polarizers; $L_{\lambda/2}$: Wave plate; L1: Plano-concave lens; L2: Bi-convex lens; L3: Cylindrical lens ($f' = +150$ mm); SB: Sliding blade; POS *xy*: *xy* micropositioner; FH: Neutral-density filter holder.

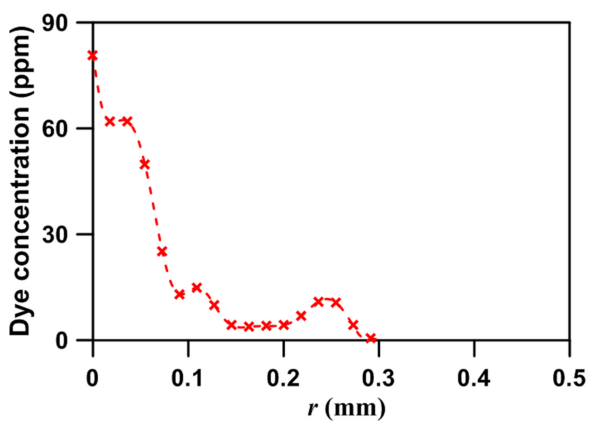


Fig. 2. Radial distribution of the dye concentration corresponding to the GI POF sample of 12-ppm.

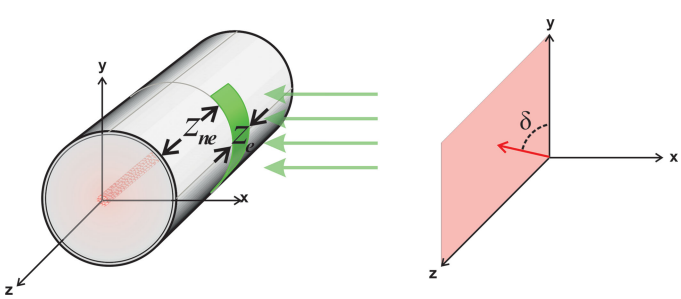


Fig. 3. Left: Illustration of the side-illumination-technique geometry showing the illuminated fiber length $z_e$, and the non-excited fiber length up to the detector $z_{ne}$. Right: Polarization angle $\delta$.

axis is defined as *y*. Due to the geometry of the excitation, the emission will be generated by the dye molecules located on the *xy* plane along the paths of the beams refracted into the fiber core. As shown in Fig. 2, the analyzed fibers have the majority of the dopant molecules placed near the fiber symmetry axis, so the main contribution to the emission will be generated by the molecules placed along those refracted beams that cross the core in close proximity to the fiber axis. These refracted beams would come from pump beams impinging on the fiber with small lateral heights y [30], [31]. Therefore, it is reasonable to assume a model in which the emission generated in the fiber is produced by dye molecules placed on the fiber axis ($x = 0, y = 0$) along the length $z_e$. On the other hand, the dye molecules in the polymer fiber can be considered as fixed and non-interacting dipoles, which preferentially absorb along the direction of their absorption transition dipole moments and emit according to their emission ones. Due to the very short propagation distances $z_{ne}$ (less than 4 cm), we have neglected the propagation losses of the emitted light. The effects of the cladding thickness in our fibers have also been ignored.

The electric-field polarization of the pump is described as a function of the polarization angle $\delta$ as follows: $\vec{E} = E_0(cos\,\delta\hat{j} + sin\,\delta\hat{k})$ (see Fig. 3). If $\delta = 0°$, the pump polarization is perpendicular to the fiber symmetry axis, i.e., $\vec{E} = E_0\,\hat{j}$, and, if $\delta = 90°$, the pump polarization is parallel to the axis, i.e., $\vec{E} = E_0\hat{k}$.

Taking all these assumptions into account, the detected emission intensity $I_e$ at the fiber end will be proportional to the following double integral over all the possible orientations of the dye molecules in the fiber ($\Omega_{mol}$) and over all the emission directions lying within the critical angle in the fiber ($\Omega$):

$$I_e(\delta) \propto T \int_{\Omega} \int_{\Omega_{mol}} P_{abs}(\delta, \Omega_{mol}) P_{emi}(\Omega_{mol}, \Omega) d\Omega_{mol} d\Omega \tag{1}$$

In this expression, $P_{abs}$ denotes the probability of pump absorption, which is proportional to the cosine squared of the angle between the pump polarization and the absorption transition

dipole moment of the molecule. $P_{emi}$ stands for the emission probability, which is proportional to the sine squared of the angle between the considered direction of emission inside the fiber and the emission transition dipole moment of the molecule. The absorption and emission transition dipole moments are considered parallel since the rhodamine 6G molecules are excited to the first singlet state [32]. *T* denotes the Fresnel transmission coefficient, which would be dependent on both the pump polarization and the lateral height in this geometry. However, this coefficient can be assumed to be constant within the approximation of small lateral heights. By working out Eq. (1) we have obtained the following expression:

$$I_e(\delta) = A + B\ cos\,(2\delta) \tag{2}$$

where *A* and *B* are positive functions dependent on the critical angle $(\theta_z)_c$, below which generated emission is guided along the fiber. The procedure for this calculation and the expressions of *A* and *B* are provided in the Appendix of this paper. An expression similar to Eq. (2) was obtained for the emitted intensity in dye-doped polymer thin films [21]. $I_e$ is maximum for $\delta = 0°$, which is the configuration corresponding to the pump polarization perpendicular to the illuminated stripe of the fiber, and $I_e$ is minimum for the polarization of the pump parallel to the stripe $(\delta = 90°)$. In order to quantify the sensitivity of the emission to the pump polarization, we use the ratio between the minimum emitted intensity and the maximum one, i.e.,:

$$\beta = \frac{(I_e)_{min}}{(I_e)_{max}} = \frac{I_e(\delta = 90°)}{I_e(\delta = 0°)} = \frac{1-(B/A)}{1+(B/A)} \tag{3}$$

As $\beta$ decreases from its maximum value $(\beta = 1)$, the influence of the pump polarization on the emitted intensity becomes stronger. The theoretical ratio $\beta$ presents a minimum value $(\beta = 1/2)$ when the emission critical angle of the fiber $(\theta_z)_c$ tends to zero and a maximum one when $(\theta_z)_c$ tends to 90° (i.e., when all emissions are guided through the fiber). As an example, Fig. 4(a) shows the theoretical variation of the emitted intensity as a function of the polarization angle estimated for a typical GI doped fiber using the critical angle for the emission at the fiber symmetry axis [28], [30].

In order to analyze the angular dependence of the emission with $\delta$, we define an average value of the sine of the axial angle for the emission emerging from the fiber. It can be determined as follows:

$$\langle sin\,\theta_z\rangle\,(\delta) = n\,(\lambda_{em}) \times \frac{\int_\Omega \int_{\Omega_{mol}} sin\theta_z P_{abs}(\delta,\Omega_{mol}) P_{emi}(\Omega_{mol},\Omega) d\Omega_{mol} d\Omega}{\int_\Omega \int_{\Omega_{mol}} P_{abs}(\delta,\Omega_{mol}) P_{emi}(\Omega_{mol},\Omega) d\Omega_{mol} d\Omega} \tag{4}$$

where the depicted magnitudes are the same as those described in Eq. (1). $n(\lambda_{em})$ is the average value of the refraction index of the fiber at the emission wavelength. By working out Eq. (4), this expression can be rewritten as follows:

$$\langle sin\,\theta_z\rangle\,(\delta) = n\,(\lambda_{em})\,\frac{C + D\,cos\,(2\delta)}{A + B\,cos\,(2\delta)} \tag{5}$$

where *A* and *B* are the positive functions of Eq. (2). The new functions *C* and *D* are also dependent on $(\theta_z)_c$. *C* is a positive

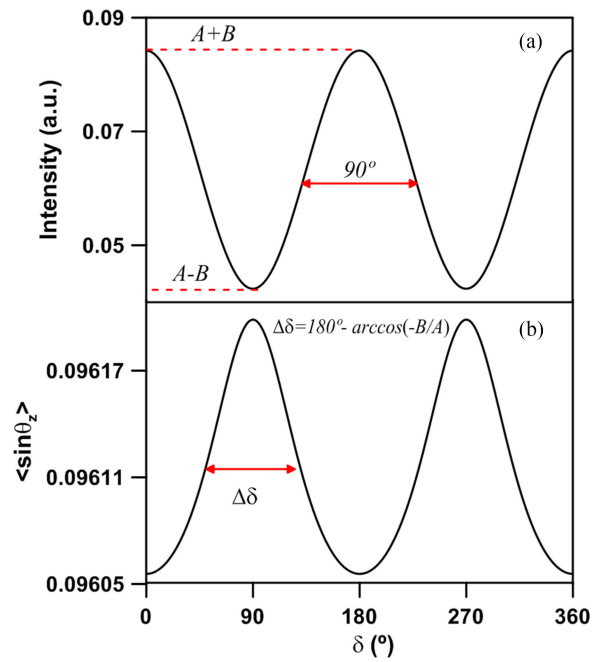


Fig. 4. (a) Emitted intensity against polarization angle. (b) Average sine of the axial angle against polarization angle. These results have been calculated employing the critical angle for the emission at the fiber symmetry axis, namely $sin\,(\theta_z)_c = (1 - (n_{clad}/\,n_{core}\,(r=0))^2)^{1/2}$, with $n_{core}\,(r=0) = 1.501$ and $n_{clad} = 1.492$.

function while *D* can be positive or negative (see the calculations in the Appendix). The theoretical variation of $<sin\,\theta_z>$ as a function of the polarization angle for a typical GI doped fiber can be seen in Fig. 4(b). Contrary to the variation of the emitted intensity with $\delta$, $<sin\,\theta_z>$ is maximum when the pump polarization is parallel to the illuminated stripe $(\delta = 90°)$, while $<sin\,\theta_z>$ is minimum for the pump polarization perpendicular to the stripe $(\delta = 0°)$. There is another difference in the curve plotted in Fig. 4(b) with respect to that shown in Fig. 4(a). Whereas the intensity curve in Fig. 4(a) has a constant width, namely $\Delta\delta = 90°$, the curve $<sin\,\theta_z>(\delta)$ in Fig. 4(b) does not present a constant width $\Delta\delta$, but it is dependent on the *A* and *B* functions. It can be demonstrated that the full width at half maximum (FWHM) of these curves is 180°$-$*arccos* $(-B/A)$. This width increases from a minimum value of 180°$-$ *arccos* $(-1/3)$ (or 70.53°) to a maximum value of 90°, corresponding to $\beta$ varying from its minimum value, i.e., $\beta = 1/2$, to its maximum one, i.e., $\beta = 1$ (see more details in the Appendix).

Although the expressions of the variation of $I_e$ and of $<sin\,\theta_z>$ with polarization angle, Eqs. (2) and (5), have been obtained for a fluorescence process, it is expected that these variations are also satisfied in an ASE regime [21].

## IV. Results and Discussion

Figure 5 illustrates the experimentally obtained polarization-angle dependence of both the emitted intensity (Figs. 5(a) and (c)) and the sine of the angle at which the emitted intensity has been reduced by half, $(sin\,\theta_z)_m$, (Figs. 5(b) and (d)). These experimental results, obtained in fluorescence and ASE regimes, correspond to the 16 ppm POF excited transversely when

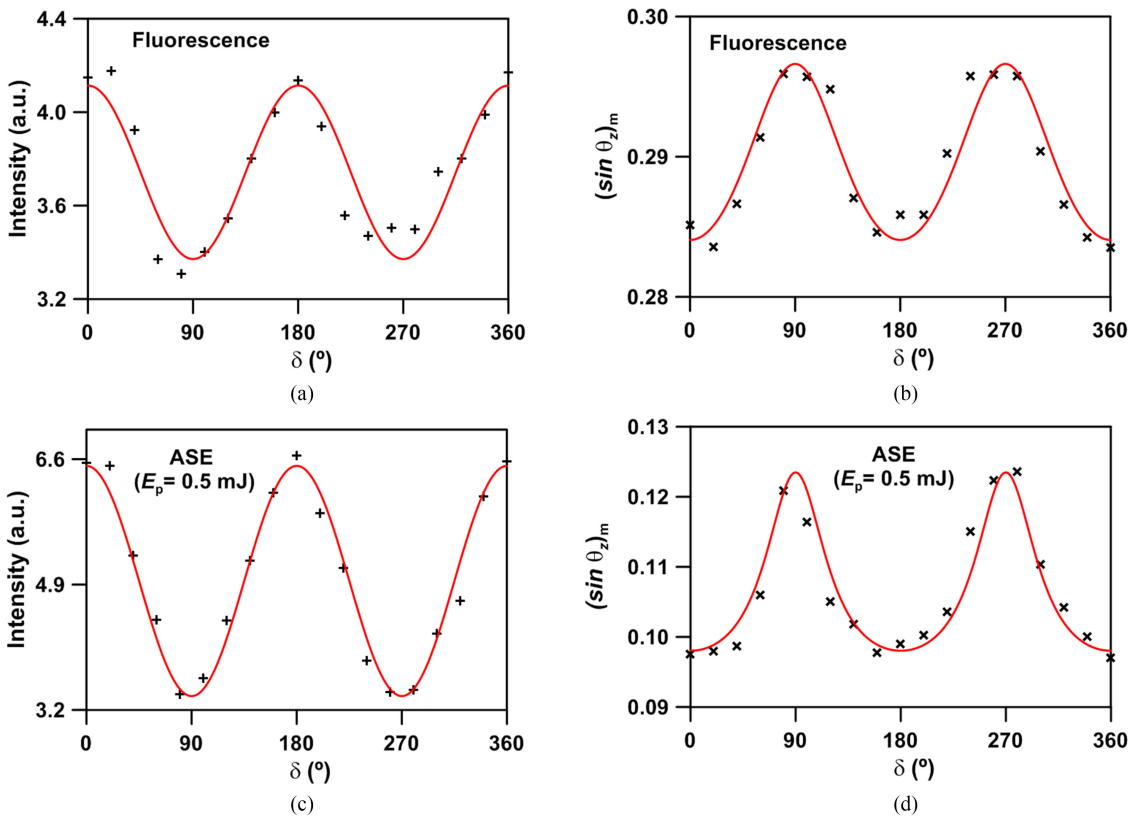


Fig. 5. (a) Fluorescence intensity and (c) ASE intensity as a function of the polarization angle. The solid lines are the fittings of Eq. (2) to the experimental points. (b) $(sin\,\theta_z)_m$ as a function of the polarization angle in the fluorescence regime and (d) in the ASE regime. The solid lines are the fittings of Eq. (5) to the experimental points. All the experimental data were obtained from the 16-ppm POF with $z_e = 0.8 \pm 0.1$ cm and $z_{ne} = 3.2 \pm 0.1$ cm.

varying the polarization angle of the pump from $\delta = 0°$ to $\delta = 360°$. In agreement with the theory shown in Section III, in both regimes the measured intensities are maximum when the pump polarization is perpendicular to the illuminated stripe (i.e., when $\delta = 0°$, 180° or 360°), and they are minimum when the polarization of the pump is parallel to the stripe or to the fiber axis (i.e., when $\delta = 90°$ or 270°). Likewise, the values of $(sin\,\theta_z)_m$ in both regimes are higher when the pump polarization is parallel to the illuminated stripe and lower when it is perpendicular to it. The higher emitted intensities and lower axial angles that are obtained for $\delta = 0°$, 180° or 360° are due to the orientation of the emission patterns of the dipole moments. For these polarization angles the majority of the excited dipole moments are aligned perpendicularly to the fiber axis and their emission patterns are mainly oriented towards the fiber symmetry axis.

Figure 6 illustrates the radiation patterns of the dipole moments aligned with both pump polarizations used. The red patterns represent the amplitude of the electric field, and the arrows on the lobes show the light radiation at the considered point. For the pump polarization perpendicular to the fiber symmetry axis, the attenuation of the emitted light tends to be lower because there are fewer multiple internal reflections of the emitted light on the core-cladding interface. This fact also contributes to the attainment of higher output intensities at the fiber end [30]. On the other hand, it can be noticed that the values of $(sin\,\theta_z)_m$ corresponding to the ASE regime are lower than those obtained in the fluorescence regime, and that the ASE curves are more jagged (see Fig. 5(b) and Fig. 5(d)). The reduction in the value of $(sin\,\theta_z)_m$ stems from the fact that the emission pattern of the molecules turns out to be more flattened in the plane perpendicular to the dipole moment when the pump energy is sufficiently increased. The variation of $(sin\,\theta_z)_m$ as the pump energy is increased has been plotted in Fig. 7, where it can be seen that the angular (axial) width of the emission is higher at low pump energies, i.e., when spontaneous emissions dominate, and it is lower at high pump energies, i.e., when ASE occurs. Notice that the drop of the emission axial width occurs at lower pump energies in the case in which the pump polarization is perpendicular to the fiber axis.

Table I shows the values of the ratio $\beta$ between the minimum and maximum intensities obtained from the fittings of the fluorescence and ASE results to Eq. (2). It also displays the widths $\Delta\delta$ of $(sin\,\theta_z)_m$ obtained from the fittings of the fluorescence and ASE results to Eq. (5). The higher value of $\beta$ obtained for the ASE regime indicates that ASE is more influenced by the pump polarization, owing to its more pronounced directional pattern. On the other hand, we have obtained that the width $\Delta\delta$ of the $(sin\,\theta_z)_m$ curves has decreased in about 26° from fluorescence to ASE measurements, indicating that the emission pattern changes more abruptly with the polarization angle when ASE occurs. It must be noticed that the values of Table I obtained for the ASE regime are very close to or exceed

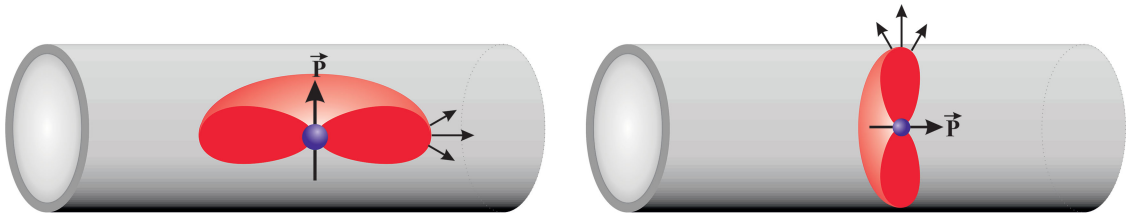


Fig. 6. Illustration of the radiation patterns for (left) a dipole perpendicular to the fiber symmetry axis and (right) a dipole parallel to fiber symmetry axis. $(\theta_z)_c$ represents the critical angle for the emission generated in the fiber.

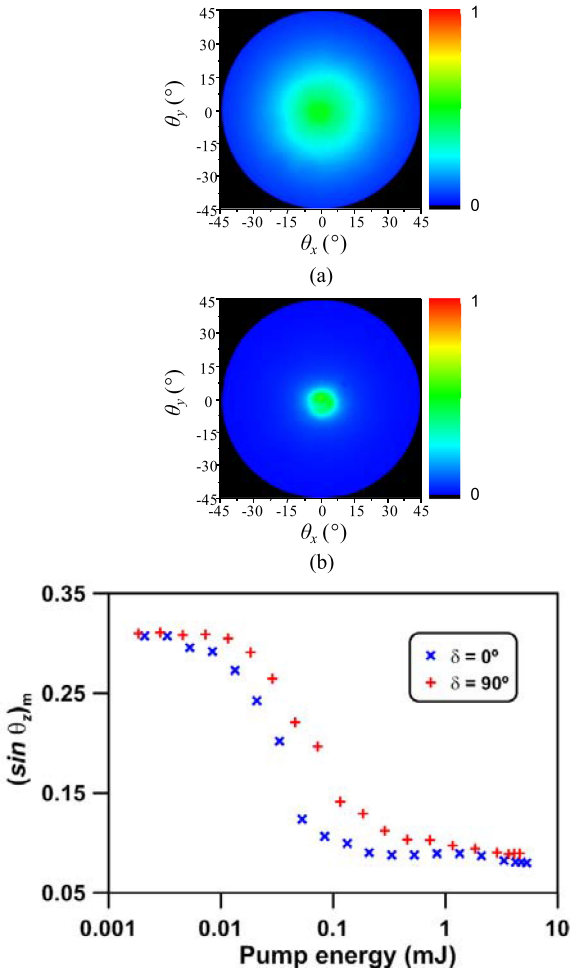


Fig. 7. Top: Images of the far-field patterns of the emission at the output of the fiber obtained with $\delta = 0°$ in the (a) fluorescence regime and in (b) ASE regime. Bottom: Experimental values of $(sin\,\theta_z)_m$ as a function of the pump energy. The results correspond to the 16-ppm POF, with $z_e = 0.8 \pm 0.1$ cm and $z_{ne} = 3.9 \pm 0.1$ cm.

TABLE I
EXPERIMENTAL VALUES OF THE RATIO $\beta$ OF THE INTENSITIES AND OF THE WIDTH $(\sin\theta_z)_m$ OF THE CURVES

| | $\beta$ | $\Delta\delta$ (°) |
|---|---|---|
| Fluorescence | $0.82 \pm 0.02$ | $78 \pm 9$ |
| ASE | $0.52 \pm 0.02$ | $52 \pm 10$ |

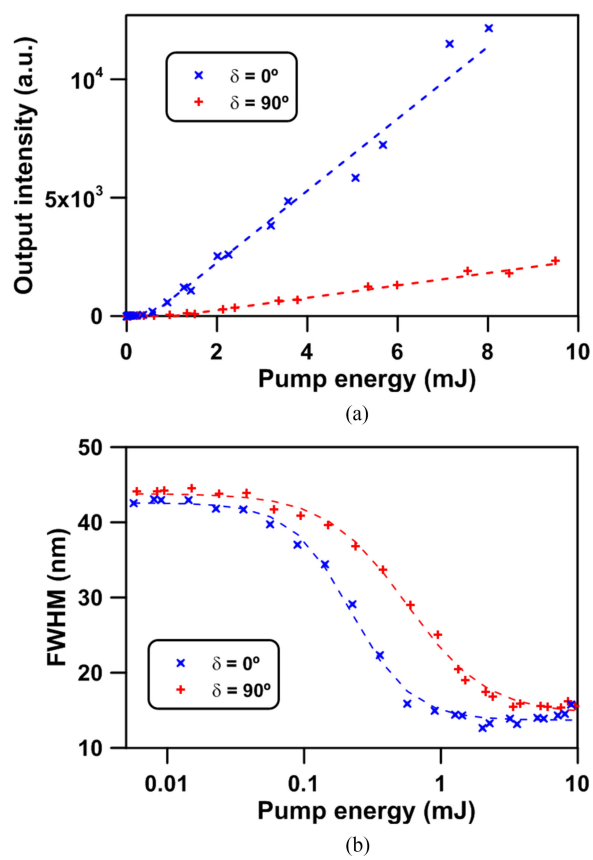


Fig. 8. (a) Output emission intensity integrated over all emission wavelengths as a function of the pump energy. The dashed lines are the linear fittings of the experimental points. (b) Narrowing of the emission spectrum as a function of the pump energy. The dashed lines are the fittings of the experimental points to a sigmoidal function. All the results correspond to the 12 ppm POF with $z_e = 1.9 \pm 0.1$ cm and $z_{ne} = 3.9 \pm 0.1$ cm. The ASE threshold is $220 \pm 20\,\mu$J with $\delta = 0°$, and $559 \pm 20\,\mu$J with $\delta = 90°$.

the theoretical minimum values of $\beta$ and $\Delta\delta$ predicted by our model. These minimum values correspond to the maximum influence of the pump polarization on the emission. Specifically, the value of $\Delta\delta$ obtained for the ASE regime is much lower than the minimum value predicted (70.53°). This discrepancy can be due mainly to the nonlinearity of the ASE process, which has not been taken into account in our model.

As can be deduced from the aforementioned results, the polarization of the pump must be perpendicular to the fiber symmetry axis in order for light to be emitted more efficiently from the fiber output end. This is corroborated in Fig. 8, which shows the experimental ASE performance in our 12 ppm POF in the case of transverse excitation for the two pump polarizations, perpendicular $(\delta = 0°)$ and parallel $(\delta = 90°)$ to the fiber symmetry

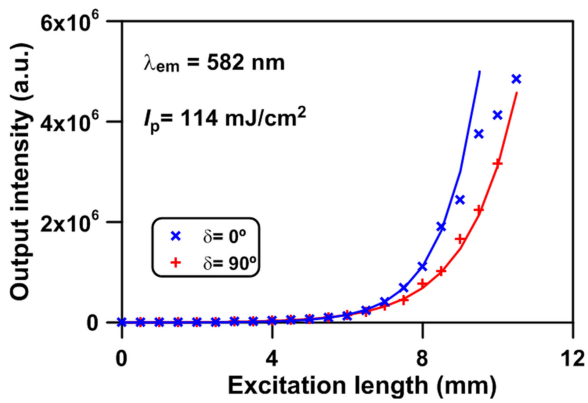


Fig. 9. Emitted intensity as a function of the excitation length. The solid lines are the fittings of Eq. (6). The results correspond to the 12-ppm POF, with $(z_e)_{\max} = 1.0 \pm 0.10$ cm and $z_{ne} = 3.9 \pm 0.1$ cm.

axis [33]. In Fig. 8(a) we have represented the total emitted intensity as a function of the pump energy. It can be noticed that the ASE threshold energy is lower for the pump polarization perpendicular to the fiber axis. Similarly, the slope of the output intensity is higher, i.e., the process is more efficient, for this pump polarization. Fig. 8(b) shows the spectral narrowing of the emission spectrum as the pump energy is increased. The drop in the FWHM can be used to determine the ASE threshold energy, for example by calculating the inflection point of a sigmoidal function that best fits the experimental points [14], [17]. As happened in Fig. 7 with the values of $(sin\,\theta_z)_m$, the drop in the FWHM also tends to occur at lower pump energies when the polarization is perpendicular to the fiber axis. These facts indicate that the ASE threshold energy is lower for this polarization, around a half in this sample.

Finally, we have calculated the ASE gains for the two polarizations ($\delta = 0°$ and 90°) by applying the VSL method. In this method, the net gain of the active fiber at the emission wavelength λ, g(λ), is obtained from the following relation between the intensity of the light emitted from the fiber end and the excitation length $z_e$:

$$I_e\left(z_e, \lambda\right) = \frac{C\left(\lambda\right)}{g\left(\lambda\right)}\left(e^{g(\lambda)z_e} - 1\right) \tag{6}$$

where C(λ) is a constant related to the spontaneous emission [18]. This equation is obtained with the assumption that the optical gain is constant along the fiber length, and it is commonly used to calculate the optical gain in active devices such as optical fibers and waveguides. In Fig. 9, we show the output intensity as a function of $z_e$ at the peak wavelength of the emission spectrum (582 nm) for a pump intensity of 114 mJ/cm$^2$ and for the two polarizations. The measurements correspond to the 12 ppm POF. As could be expected, we can see a greater increase of the intensity with excitation length when the pump polarization is perpendicular to the fiber symmetry axis. By fitting Eq. (6) to the experimental points we obtain, for this fiber, that the optical gain for the perpendicular polarization is $9.9 \pm 0.3\,\text{cm}^{-1}$, i.e., around 1.3 times higher than that obtained for the parallel polarization ($7.6 \pm 0.1\,\text{cm}^{-1}$). We have obtained similar ratios between the gains for the perpendicular and parallel polarizations when pumping the fiber with other intensities. As can be seen, the polarization of the pump beam impinging transversely on dye doped POFs has a great effect on the values of the threshold energies and optical gains. With the experimental set-ups employed, no noticeable degree of polarization of the light emerging from the fiber was detected, neither in fluorescence regime nor in ASE one.

## V. Conclusions

In this paper, we have demonstrated that the polarization of the pump has a great effect on the properties of the emission generated in a graded-index polymer optical fiber doped with rhodamine 6G when the fiber is pumped from its side. On the one hand, we have theoretically and experimentally studied the influence of the pump polarization on the emission intensity and on the angular axial distribution emerging from the fiber end. We have developed a simple model that shows that, when the pump polarization is perpendicular to the fiber symmetry axis, the emission intensity is higher and the angular distribution is narrower around the fiber symmetry axis as compared with the case of the parallel pump polarization. On the other hand, we have experimentally shown that the properties of the amplified spontaneous emission, such as its threshold-like energy, relative efficiency and gain, are strongly dependent on the pump polarization. Particularly, for the doped fiber with an average concentration of 12 ppm, we have demonstrated that the threshold energy is lower (around a half) and that the gain is higher (around 1.3 times) when the pump polarization is perpendicular to the fiber symmetry axis. In summary, the pump polarization must be carefully controlled in order to optimize the emission performance of dye doped polymer optical fibers when they are transversely pumped. These results can be useful for the manufacture of photonic devices and sensor elements that are based on doped polymer optical fibers.

## Appendix

Using the axis depicted in Fig. 3, the absorption dipole moment of the molecule for any orientation is written as:

$$\vec{p}_{abs} = p_{abs}(sin\,\alpha cos\,\varphi\,\hat{i} + sin\,\alpha sin\,\varphi\hat{j} + cos\,\alpha\hat{k}) \tag{A.1}$$

where $\alpha$ is the angle made by $\vec{p}_{abs}$ with the fiber symmetry axis ($z$-axis), and $\varphi$ is the angle of $\vec{p}_{abs}$ relative to the $x$-axis in the $xy$ plane. Therefore, the probability of pump absorption $P_{abs}$, which is proportional to the cosine squared of the angle between the pump polarization $\vec{E} = E_0(cos\,\delta\hat{j} + sin\,\delta\hat{k})$ (see Fig. 3) and the dipole moment $\vec{p}_{abs}$ of the molecule, is expressed as:

$$P_{abs} \propto ((sin\,\alpha sin\,\varphi cos\,\delta) + (cos\,\alpha sin\,\delta))^2 \tag{A.2}$$

Likewise, the emission probability $P_{emi}$, which is proportional to the sine squared between the direction of the emission inside the fiber:

$$\hat{e} = (sin\,\theta_z cos\,\phi_x\,\hat{i} + sin\,\theta_z sin\,\phi_x\hat{j} + cos\,\theta_z\hat{k}) \tag{A.3}$$

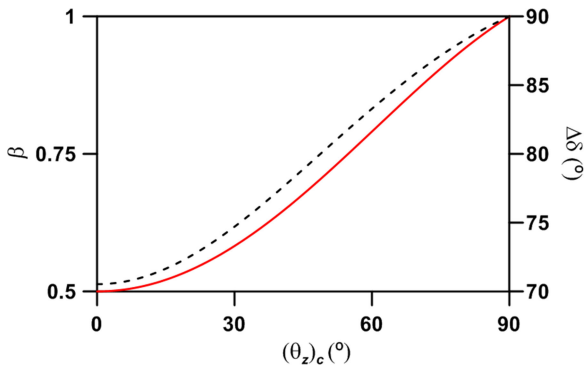


Fig. 10. Theoretical values of the ratio $\beta$ (solid line) and of the width $\Delta\delta$ (dashed line) as functions of $(\theta_z)_c$.

and the emission dipole moment of the molecule, in our case parallel to $\vec{p}_{abs}$, is given by:

$$P_{emi} \propto 1 - ((sin\,\alpha cos\,\varphi sin\,\theta_z cos\,\phi_x) + \\ + (sin\,\alpha sin\,\varphi sin\,\theta_z sin\,\phi_x) + (cos\,\alpha cos\,\theta_z))^2 \quad (A.4)$$

Here $\theta_z$ is the angle made by $\hat{e}$ with the fiber symmetry axis, whereas $\phi_x$ describes the angle of $\hat{e}$ relative to the *x*-axis in the *xy* plane.

Taking the expressions shown above and Eq. (1) into account, the emitted intensity $I_e$ as a function of the polarization angle is calculated by means of the following integrals:

$$I_e(\delta) \propto \int_0^{(\theta_z)_c} sin\,\theta_z d\theta_z \int_0^{2\pi} d\phi_x \\ \times \int_0^{\pi} sin\,\alpha d\alpha \int_0^{2\pi} P_{abs}(\alpha,\varphi,\delta) P_{emi}(\alpha,\varphi,\theta_z,\phi_x) d\varphi \quad (A.5)$$

where all the possible orientations of the dye molecules and all the emission directions lying within the critical angle of the emission $(\theta_z)_c$ have been taken into account. The calculation of this integral leads to the following expression:

$$I_e(\delta) = A + B\,cos\,(2\delta) \quad (A.6)$$

with

$$A\,((\theta_z)_c) = \frac{16\pi^2}{9} - \frac{9}{5}\pi^2 cos\,(\theta_z)_c + \frac{\pi^2}{45} cos\,3(\theta_z)_c \quad (A.7)$$

$$B\,((\theta_z)_c) = \frac{\pi^2}{15} cos\,(\theta_z)_c - \frac{1}{15}\pi^2 cos\,3(\theta_z)_c \quad (A.8)$$

The ratio $\beta$ between $(I_e)_{\min}$ and $(I_e)_{\max}$ can be expressed as a function of $(\theta_z)_c$ as follows:

$$\beta\,((\theta_z)_c) = \frac{(I_e)_{min}}{(I_e)_{max}} = -2 + \frac{60}{21 + 2cos(\theta_z)_c + cos2(\theta_z)_c} \quad (A.9)$$

Figure 10 shows the variation of the theoretically calculated values of $\beta$ as a function of $(\theta_z)_c$ from its minimum value ($\beta = 1/2$) to its maximum one ($\beta = 1$). As $(\theta_z)_c$ increases, more emissions are guided along the fiber, and the influence of the pump polarization on the emission becomes smaller.

The average value of the sine of the axial angle for the emission emerging from the fiber end is calculated from Eq. (4) in the same way as shown in Eq. (A.5). The calculations of the integrals provide the following expression:

$$\langle sin\,\theta_z \rangle\,(\delta) = n\,(\lambda_{em})\,\frac{C + D\,cos\,(2\delta)}{A + B\,cos\,(2\delta)} \quad (A.10)$$

with

$$C\,((\theta_z)_c) = \frac{9\pi^2}{10}(\theta_z)_c - \frac{7\pi^2}{15} sin\,2(\theta_z)_c + \frac{\pi^2}{120} sin\,4(\theta_z)_c \quad (A.11)$$

$$D\,((\theta_z)_c) = -\frac{\pi^2}{30}(\theta_z)_c + \frac{\pi^2}{15} sin\,2(\theta_z)_c - \frac{\pi^2}{40} sin\,4(\theta_z)_c \quad (A.12)$$

and *A* and *B* are given by Eq. (A.7) and Eq. (A.8), respectively.

The full width at half maximum, $\Delta\delta$, of the curve of $< sin\,\theta_z >$ as a function of the polarization angle only depends on the functions *A* and *B*, and it is given by:

$$\Delta\delta\,((\theta_z)_c) = 180^\circ - arccos\left(-\frac{B}{A}\right) \quad (A.13)$$

or, equivalently,

$$\Delta\delta\,((\theta_z)_c) \\ = 180^\circ - arccos\left(-\frac{6sin\,(\theta_z)_c sin\,2(\theta_z)_c}{80 - 81cos\,(\theta_z)_c + cos\,3(\theta_z)_c}\right) \quad (A.14)$$

The variation of $\Delta\delta$ with $(\theta_z)_c$ has been included in Fig. 10. Similarly to the ratio $\beta$ , $\Delta\delta$ increases from its minimum value ($\Delta\delta = 180^\circ - arccos\,(-1/3)$), obtained when $(\theta_z)_c$ tends to 0°, to a maximum value ($\Delta\delta = 90^\circ$), obtained when $(\theta_z)_c$ tends to 90°.

Notice that the theoretical expressions for *A*, *B*, *C*, *D*, $\beta$ and $\Delta\delta$ are only applicable when the angle between the absorption and emission transition dipoles of the dopant molecule is nearly 0, as happens in the case of the dye rhodamine 6G. The value of this angle depends on the molecular structure of the dye, and in the general case, it would appear in the theoretical expressions as the argument of a cosine.

## References


[1] J. Clark and G. Lanzani, "Organic photonics for communications," *Nat. Photon.*, vol. 4, pp. 438–446, Jul. 2010.

[2] J. Arrue, F. Jiménez, I. Ayesta, M.A. Illarramendi, and J. Zubia, "Polymer-optical-fiber lasers and amplifiers doped with organic dyes," *Polymers*, vol. 3, no. 3, pp. 1162–1180, Jul. 2011.

[3] K. Peters, "Polymer optical fiber sensors—A review," *Smart Mater. Struct.*, vol. 20, no. 1, Jan. 2011, Art. no. 013002.

[4] S. Kamimura and R. Furukawa, "Strain sensing based on radiative emission-absorption mechanism using dye-doped polymer optical fiber," *Appl. Phys. Lett.*, vol. 111, no. 6, Aug. 2017, Art. no. 063301.

[5] I. Parola *et al.*, "Fabrication and characterization of polymer optical fibers doped with perylene-derivatives for fluorescent lighting applications," *Fibers*, vol. 5, no. 3, Sep. 2017, Art. no. 28.

[6] Y. Koike, *Fundamentals of Plastic Optical Fibers*. Weinheim, Germany: Wiley-VCH, 2015.

[7] M. G. Kuzyk, *Polymer Fiber Optics: Materials, Physics, and Applications*. Boca Raton, FL, USA: CRC Press, 2007.

[8] J. Xu *et al.*, "Exploration in performance scaling and new application avenues of superfluorescent fiber source," *IEEE J. Sel. Topics Quantum Electron.*, vol. 24, no. 3, May/Jun. 2018, Art. no. 0900710.

[9] J. Bonefacino, X. Cheng, M. L. V. Tse, and H. Y. Tam, "Recent progress in polymer optical fiber light sources and fiber Bragg gratings," *IEEE J. Sel. Topics Quantum Electron.*, vol. 23, no. 2, Mar./Apr. 2017, Art. no. 5600911.

[10] B. Redding, P. Ahmadi, V. Mokan, M. Seifert, M. A. Choma, and H. Cao, "Low-spatial-coherence high-radiance broadband fiber source for speckle free imaging," *Opt. Lett.*, vol. 40, no. 20, pp. 4607–4610, Oct. 2015.

[11] H. C. Lefevre, *The Fiber-Optic Gyroscope*. Norwood, MA, USA: Artech House, 2014.

[12] G. Morello, M. Moffa, S. Girardo, A. Camposeo, and D. Pisignano, "Optical gain in the near infrared by light-emitting electrospun fibers," *Adv. Funct. Mater.*, vol. 24, no. 33, pp. 5225–5231, Sep. 2014.

[13] A. Camposeo, L. Persano, and D. Pisignano, "Light-emitting electrospun nanofibers for nanophotonics and optoelectonics," *Macromol. Mater. Eng.*, vol. 298, no. 5, pp. 487–503, May 2013.

[14] M. A. Illarramendi *et al.*, "Amplified spontaneous emission in graded-index polymer optical fibers: Theory and experiment," *Opt. Express*, vol. 21, no. 20, pp. 24254–24266, Oct. 2013.

[15] G. V. Maier *et al.*, "Active polymer fibres doped with organic dyes: Generation and amplification of coherent radiation," *Quantum Electron.*, vol. 37, no. 1, pp. 53–59, 2007.

[16] K. Kuriki, T. Kobayashi, N. Imai, T. Tamura, Y. Koike, and Y. Okamoto, "Organic dye-doped polymer optical fiber laser," *Polym. Adv. Technol.*, vol. 11, no. 8–12, pp. 612–616, Aug./Dec. 2000.

[17] J. Arrue *et al.*, "Laser-like performance of side-pumped dye-doped polymer optical fibers," *IEEE Photon. J.*, vol. 7, no. 2, Apr. 2015, Art. no. 7100611.

[18] I. Parola *et al.*, "Characterization of the optical gain in doped polymer optical fibres," *J. Lumin.*, vol. 177, pp. 1–8, Sep. 2016.

[19] R. J. Kruhlak and M. G. Kuzyk, "Side-illumination fluorescence spectroscopy. I. Principles," *J. Opt. Soc. Amer. B*, vol. 16, no. 10, pp. 1749–1755, Oct. 1999.

[20] K. L. Shaklee and R. F. Leheny, "Direct determination of optical gain in semiconductor crystals," *Appl. Phys. Lett.*, vol. 18, no. 11, Jun. 1971, Art. no. 475.

[21] I. Gozhyk *et al.*, "Gain properties of dye-doped polymer thin films," *Phys. Rev. B*, vol. 92, Dec. 2015, Art. no. 214202.

[22] I. Gozhyk *et al.*, "Polarization properties of solid-state organic lasers," *Phys. Rev. A*, vol. 86, Oct. 2012, Art. no. 043817.

[23] E. K. Keshmarzi, R. N. Tait, and P. Berini, "Near infrared amplified spontaneous emission in a dye-doped polymeric waveguide for active plasmonic applications," *Opt. Express*, vol. 22, no. 10, pp. 12452–12460, May 2014.

[24] S. V. Frolov, M. Shkunov, Z. V. Vardeny, and K. Yoshino, "Ring microlasers from conducting polymers," *Phys. Rev. B*, vol. 56, no. 8, Aug. 1997, Art. no. R4363(R).

[25] J. Wang and K. Y. Wong, "Polarization characteristics of a light-emitting polymer microring laser," *Appl. Phys. B*, vol. 87, no. 4, pp. 685–691, Jun. 2007.

[26] T. Ben-Messaoud *et al.*, "Longitudinal pumping of polymer microring lasers," *Synth. Met.*, vol. 127, no. 1–3, pp. 159–163, Mar. 2002.

[27] M. Aslund, S. D. Jackson, J. Canning, A. Teixeira, and K. Lyytikainen-Digweed, "The influence of skew rays on angular losses in air-clad fibres," *Opt. Commun.*, vol. 262, no. 1, pp. 77–81, Jun. 2006.

[28] I. Bikandi, M. A. Illarramendi, J. Zubia, J. Arrue, and F. Jiménez, "Side-illumination fluorescence critical angle: Theory and application to F8BT-doped polymer optical fibers," *Opt. Express*, vol. 20, no. 4, pp. 4630–4644, Feb. 2012.

[29] Y. Koike, I. Ishigure, and E. Nihei, "High-bandwidth graded-index polymer optical fiber," *J. Lightw. Technol.*, vol. 13, no. 7, pp. 1475–1489, Jul. 1995.

[30] A. W. Snyder and J. D. Love, *Optical Waveguide Theory*. New York, NY, USA: Springer-Verlag, 1983.

[31] M. A. Illarramendi, G. Aldabaldetreku, I. Bikandi, J. Zubia, G. Durana, and A. Berganza, "Scattering in step-index polymer optical fibers by side-illumination technique: Theory and application," *J. Opt. Soc. Amer. B*, vol. 29, no. 6, pp. 1316–1329, Jun. 2012.

[32] B. Valeur and M. N. Berberan-Santos, *Molecular Fluorescence: Principles and Applications*, 2nd ed. Weinheim, Germany: Wiley-VCH, 2012.

[33] M. A. Illarramendi, J. Arrue, J. Zubia, I. Bikandi, A. Tagaya, and Y. Koike, "Polarization properties in doped polymer optical fibers," in *Proc. 23rd Int. Conf. Plastic Opt. Fibers*, Yokohama, Japan, 2014, pp. 140–143.

Authors' biographies not available at the time of publication.